in vivo *38*: 1064-1073 (2024)
doi:10.21873/invivo.13540

Acute Myelomonoblastic Leukemia (My1/De): A Preclinical Rat Model

VIKTÓRIA ARATÓ[1,2,#], ZITA KÉPES[1,#], JUDIT P. SZABÓ[1], GERGELY FARKASINSZKY[1], TAMÁS SASS[3], NOÉMI DÉNES[1], ADRIENN KIS[1], GÁBOR OPPOSITS[1], ISTVÁN JÓSZAI[1], FERENC KRISZTIÁN KÁLMÁN[4], ISTVÁN HAJDU[1], GYÖRGY TRENCSÉNYI[1] and ISTVÁN KERTÉSZ[1,2]

[1]*Division of Nuclear Medicine and Translational Imaging, Department of Medical Imaging, Faculty of Medicine, University of Debrecen, Debrecen, Hungary;*
[2]*Doctoral School of Pharmaceutical Sciences, University of Debrecen, Debrecen, Hungary;*
[3]*Department of Surgery, Faculty of Medicine, University of Debrecen, Debrecen, Hungary;*
[4]*Department of Physical Chemistry, University of Debrecen, Debrecen, Hungary*

Abstract. *Background/Aim: Since acute myeloid leukemias still represent the most aggressive type of adult acute leukemias, the profound understanding of disease pathology is of paramount importance for diagnostic and therapeutic purposes. Hence, this study aimed to explore the real-time disease fate with the establishment of an experimental myelomonoblastic leukemia (My1/De) rat model using preclinical positron emission tomography (PET) and whole-body autoradiography. Materials and Methods: In vitro [^{18}F]F-FDG uptake studies were performed to compare the tracer accumulation in the newly cultured My1/De tumor cell line (blasts) with that in healthy control and My1/De bone marrow suspensions. Post transplantation of My1/De cells under the left renal capsule of Long-Evans rats, primary My1/De tumorigenesis, and metastatic propagation were investigated using [^{18}F]F-FDG PET imaging, whole-body autoradiography and phosphorimage analyses. To assess the organ uptake profile of the tumor-carrying animals we accomplished ex vivo biodistribution studies. Results: The tracer accumulation in the My1/De culture cells exceeded that of both the tumorous and the healthy bone marrow suspensions ($p<0.01$). Based on in vivo imaging, the subrenally transplanted My1/De cells resulted in the development of leukemia in the abdominal organs, and metastasized to the mesenterial and thoracic parathymic lymph nodes (PTLNs). The lymphatic spread of metastasis was further confirmed by the significantly higher %ID/g values of the metastatic PTLNs (4.25±0.28) compared to the control (0.94±0.34). Cytochemical staining of the peripheral blood, autopsy findings, and wright-Giemsa-stained post-mortem histological sections proved the leukemic involvement of the assessed tissues/organs. Conclusion: The currently established My1/De model appears to be well-suited for further leukemia-related therapeutic and diagnostic investigations.*

Even though recent decades witnessed great advancements in understanding the pathological processes of acute myeloid leukemia (AML), this hematologic malignancy still remains the most aggressive type of adult acute leukemia (1). Owing to their inherent ability to resemble primary tumorigenesis and metastatic spread, preclinical leukemic models hold great promise in revealing clinically relevant complementary information on AML-associated genetic, cellular as well as immunological abnormalities.

Despite the seamless maintenance and negligible costs of murine models (2), given that rats are physiologically, genetically, and morphologically more similar to humans than mice, rat-based rodent models appear to be superior to murine ones for oncological trials (3). Additionally, the greater dimensions of rats not only favour the easy performance of micro-interventions or tissue sampling (3), but also allow for the identification of smaller lesions such as metastases. Due

[#]These Authors contributed equally to this study.

Correspondence to: Dr. Zita Képes, Division of Nuclear Medicine and Translational Imaging, Department of Medical Imaging, Faculty of Medicine, University of Debrecen, Nagyerdei St. 98, H-4032 Debrecen, Hungary. Tel: +36 (70)3646025, e-mail: kepes.zita@med.unideb.hu

Key Words: 2-deoxy-2-[^{18}F]fluoro-D-glucose ([^{18}F]F-FDG), metastasis, myelomonoblastic leukemia (My1/De), parathymic lymph node, (PTLN), preclinical, positron emission tomography (PET), whole-body autoradiography.

to the greater genomic closeness of rats to humans compared to mice (4), rat models are also well-suited to test the efficacy and safety profile of drug-to-be molecules.

Induced by viral infection, irradiation, and different chemicals/pollutants, rat leukemic systems were successfully proposed to assess disease fate, treatment response or leukemia-related molecular characteristics (5-10). Furthermore, experimental models recapitulating AML uncovered much about the molecular pathophysiology (11, 12) and the therapeutic approaches of the disease (13-15). Considering the largely comparable myeloid features of subcutaneously transplanted Wistar/Furth (W/Fu) AML (16) or 7, 12-dimethylbenz(a)anthracene (DMBA)-generated acute rat leukemia (17) to those of the human disease, AML models could also be applicable for the evaluation of anti-tumor drug candidates prior to clinical usage.

Nuclear medical techniques including positron emission tomography (PET) provide unique opportunity to obtain correct representation of the primary tumor formation and metastatic spread of *in vivo* developed leukemias (18). [^{18}F]F-FDG or [^{11}C]C-methionine PET imaging proved the metastatic potential of My2/De *(*isolated at the University of Debrecen/De*)* myelomonoblastic leukemia cells to the thoracic parathymic lymph nodes (PTLNs) in corresponding tumor-bearing Long-Evans rats (18). As far as we are aware, no prior studies dealt with the *in vivo* assessment of another type of myelomonoblastic leukemia – denoted as My1/De – therefore, we currently aimed at exploring its real-time propagation in inbred My1/De xenotransplanted Long-Evans rats using preclinical PET imaging and whole-body autoradiography. Additional interest was placed upon the comparison of the [^{18}F]F-FDG uptake mechanism in healthy and My1/De leukemic bone marrow cells.

Materials and Methods

Animal handling. Inbred female Long-Evans rats (n=20) ranged in weight from 150 to 200 g were housed under conventional laboratory conditions with semi-synthetic food (Charles River Ltd., Gödöllő, Hungary) and water ad libitum and 12-hour light-dark cycle. To ensure animal welfare, the rats were daily observed by experienced laboratory assistants. The examinations and animal handling were in line with the 3R principles and criteria established in the UK "Guide for the Care and Use of Laboratory Animals" (19). All experiments were conducted according to the rules and regulations of the Animal Experimentation Committee of the UK (19) and approved by the Ethics Committee for Animal Experimentation of the University of Debrecen (study number: 21/2017/DEMÁB).

Tumor development. Myelomonoblastic leukaemia was induced in female 50-day-old Long-Evans rats by the intravenous injection of 3×40 mg/kg 7,12-dimethylbenz[a]anthracene (DMBA) solution based on the previously described methods of Huggins and Sugiyama (6). This treatment was conducted once in three consecutive weeks and after 9 months the My1/De tumor developed. As mentioned formerly, the abbreviation of the leukemic cells stands for myelomonoblastic leukemia 1 isolated at the University of Debrecen. Thereafter, the tumorous enlarged spleen was removed, sliced into smaller pieces, and the fragments were serially transplanted under the left renal capsule of the Long-Evans rats or stored in liquid nitrogen.

Subrenal capsule assay – SRCA. Subrenal capsule assay method (SRCA) (20) was applied for the transplantation of a piece of rat-derived monoblastic sarcoma tumor, and 10^6 My1/De myelomonoblastic cells under the left renal capsule of the experimental animals to follow the *in vivo* metastatic route of the leukemic cells. The experimental operation was in accordance with the process described earlier in detail by Képes and Trencsényi (21). Briefly, the rats were anaesthetised with 1,5% Forane (AbbVie, Budapest, Hungary; OGYI-T-1414/01). Followed by the shaving and the disinfection of the left lumbar region, the retroperitoneum was opened by a lumbar incision, and the tumor fragments or cells placed on Gelaspon^R disc in 10 μl saline were inoculated under the renal capsule of the exposed left kidney. Thereafter, the skin and the muscle layer were closed using surgical stitches and staples. The autopsy and all experiments were performed a month later.

Establishment of My1/De tumor cell line. For the generation of My1/De cell cultures, Long-Evans rats with a minimum of 70-100 g/l white blood cell (WBC) count were used. The cell isolation process was performed according to the methods of Trencsényi *et al*. (18). Briefly, forane-based over anaesthetisation was followed by the extraction of the myelomonoblastic sarcoma tumors and the thigh bones. After having the bone ends cut off and cleared, the inside of the femoral tube was withdrawn and washed with sterile physiological saline solution. The bone marrow was suspended with sterile pipette, then after centrifugation for 5 min (400 g) the cell suspension was taken up in RPMI 1640 culture medium containing 10% FBS and antibiotic solution and was cultured at 37˚C in a 5% CO_2 atmosphere. The adherent cells were disposed, while we cultured the non-adherent subtypes for additional three days. Trypan blue exclusion test was applied for the determination of the number of the viable tumor cells used for the experiments. It took four days for the cells to develop into macrophages.

[^{18}F]F-FDG uptake measurements. Radiopharmaceutical synthesis. 2-[^{18}F]Fluoro-2-deoxy-D-glucose ([^{18}F]F-FDG) PET radiopharmaceutical was produced at the Division of Nuclear Medicine and Translational Imaging, Department of Medical Imaging, Faculty of Medicine, University of Debrecen (Debrecen, Hungary).

Measurement of in vitro [^{18}F]F-FDG uptake. In vitro [^{18}F]F-FDG uptake measurements were performed using bone marrow cells freshly isolated from healthy and My1/De leukemic rats, and cells derived from a 20-day-old blast culture from bone marrow suspension. The applied bone marrow suspension derived from such leukemic rats whose peripheral WBC count was 60-80 g/l instead of the physiological 6-7 g/l, with 70-80% of blast cells. The radiopharmaceutical uptake kinetics were assessed at three time points, 15-, 30-, and 60-min post incubation.

The cell suspensions of both control and leukemic bone marrow (1×10^6/ml) were pre-incubated for 10 min in 5 mM D-glucose containing PBS at 36˚C, then 0.37 MBq of [^{18}F]F-FDG were added

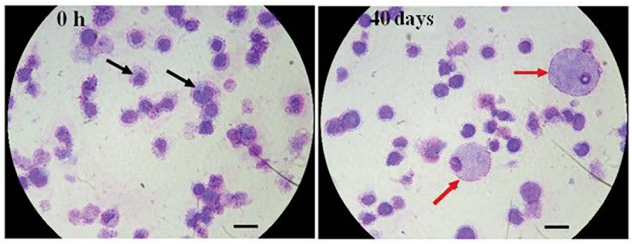

Figure 1. *Demonstration of the differentiation of the leukemic blast cells into macrophages (black arrows: blast cells, red arrows: macrophages; indication: 10 μm) (Original magnification ×400).*

to the samples. The cells were further incubated with [^{18}F]F-FDG for the time predetermined in the experiments. After the suppression of the radiopharmaceutical uptake with cold PBS, the same solution was used for the cleanse of the cells. Calibrated gamma counter (Perkin-Elmer Packard 406 Cobra, Waltham, MA, USA) was used for cell radioactivity determination, and the decay-corrected radiopharmaceutical accumulation was calculated in units of counts per minute (10^6 cell)$^{-1}$ [cpm]. The amount of cellular [^{18}F]F-FDG accumulation was also expressed as the percentage of the incubating dose (ID%) that reflects what percentage of the [^{18}F]F-FDG activity in the external incubation solution is taken up by one million cells.

MiniPET studies. To perform *in vivo* uptake studies, 14 days after My1/De cell inoculation, 15 MBq of [^{18}F]F-FDG were intravenously administered into the lateral tail vein of the leukemic rats. Sixty minutes post radiotracer injection, 10-min whole-body static PET images were acquired on all animals with MiniPET-II small animal PET device (Division of Nuclear Medicine and Translational Imaging, Department of Medical Imaging, Faculty of Medicine, University of Debrecen, Debrecen, Hungary).

Isoflurane-induced anaesthesia using 3% and 1.5% forane for anaesthesia induction and maintenance respectively (AbbVie, 0.4 l/min O_2 Linde Healthcare, Budapest, Hungary; OGYI-T-20607), and 1.2 l/min N_2O (Linde Healthcare; OGYI-T-21090) was maintained throughout the whole imaging process.

As part of PET data assessment, three-dimensional ellipsoidal volumes of interest (VOIs) were carefully placed around the edge of the radioactivity of selected organs/tissues to quantify their radiopharmaceutical concentration using the BrainCad image analysis software (University of Debrecen, Debrecen, Hungary). The radioactivity of the regions concerned was expressed in standardised uptake values (SUV).

Organ distribution studies. To assess the radiopharmaceutical uptake pattern of the animals, two weeks after tumor transplantation *ex vivo* biodistribution studies were conducted both in the healthy and My1/De tumor-bearing rats.

Fifteen MBq of [^{18}F]F-FDG were intravenously injected into the later tail vein of the study rats, then after one hour long tracer distribution time forane-based euthanasia was applied. Blood sample was taken from the aorta, and the following selected organs and tissues were harvested and weighed: spleen, kidneys, liver, muscle, the tumor itself and the metastatic PTLN. Gamma-counting was used for radioactivity measurement. The weight and the radiotracer concentration of the samples were presented in %ID/g.

A

	15 min	30 min	60 min
Control bone marrow	0.10 ± 0.10	0.24 ± 0.12	0.49 ± 0.16
My1/De bone marrow	0.30 ± 0.10	0.60 ± 0.20	1.20 ± 0.19
My1/De cells	0.85 ± 0.37	1.88 ± 0.33	3.39 ± 0.88

B

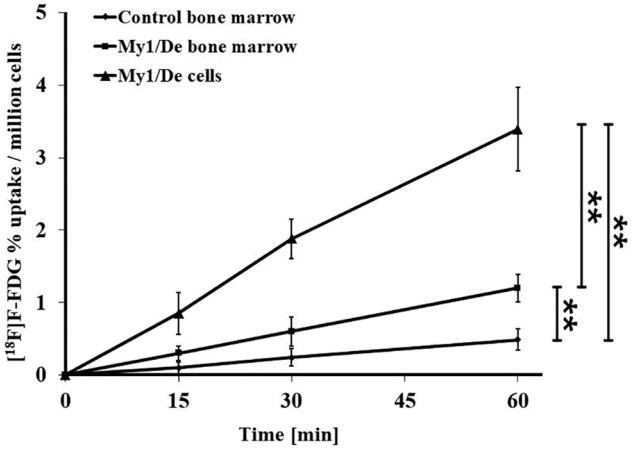

Figure 2. *In vitro [^{18}F]F-FDG uptake measurements. [^{18}F]F-FDG accumulation in control bone marrow cells, myelomonoblastic leukemia 1 isolated at the University of Debrecen (My1/De) bone marrow cells. and My1/De blast cells 15, 30, and 60 min post incubation (Panel A). The radiotracer uptake was determined using a calibrated γ counter, and the uptake values are presented in (%ID/g)±SD. Time-activity curve demonstrating the [^{18}F]F-FDG uptake kinetics of the control bone marrow cells, My1/De bone marrow cells and My1/De blast cells 15, 30, and 60 min post incubation (Panel B). Significance level between the cell groups at each investigated time point: p≤0.01 (**).*

Whole-body autoradiography. Followed by the intravenous injection of 15 MBq of [^{18}F]F-FDG into the left tail vein of the control and tumor-carrying rats, the animals were terminated (5% Forane), embedded into 1% carboxymethyl cellulose solution and frozen in liquid nitrogen. Sagittal 60 micron thick histological sections were prepared from the blocks containing the embedded animals at -20^{O}C using Leica CM 3600 cryomacrotome (Leica Biosystems, Nussloch, Germany). Parallel with the exposure of the sections on PhosphorImager discs (GE Healthcare, Piscatway, NJ, USA), colour pictures were taken for the identification of the anatomical structures with a HP ScanJet 4cT transparency scanner (Hewlett-Packard, Palo Alto, CA, USA). The software-based registration of the autoradiographic images and the transparency pictures allows for the fusion of the anatomical and the functional information. As part of the phosphorimage analysis, regions of interest (ROIs) were placed on predefined anatomical regions to calculate their relative intensity values from the average of 16 slices applying the Image Quant™ TL 1.5 (GE Healthcare) software.

Wright-Giemsa staining. Smears were prepared from the tumorous spleen, bone marrow, PTLN and from the peripheral blood of the leukemic rats. Giemsa dye was used to stain the smears according to the manufacturer's instructions (Sigma-Aldrich, Budapest, Hungary).

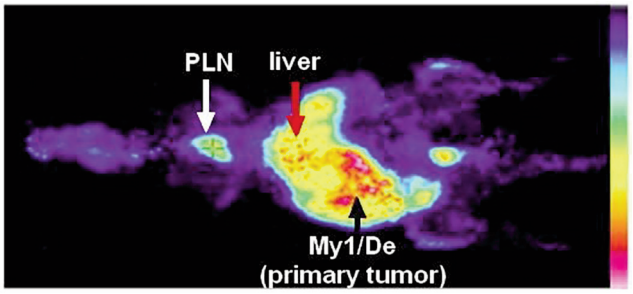

Figure 3. *Representative [18F]F-FDG positron emission tomography image of a myelomonoblastic leukemia 1 isolated at the University of Debrecen (My1/De) tumor-bearing Long-Evans rat. In vivo static miniPET images were acquired two weeks after tumor cell inoculation and 60 min post intravenous injection of 15 MBq of [18F]F-FDG with a preclinical PET device. The subrenally growing primary tumor occupies meaningful territory in the abdominal cavity (black arrow). The tumor-associated enlargement of the parathymic lymph node, and the liver is indicated by the white, and red arrows, respectively.*

Statistical analyses. MedCalc 18.5 software package was used for the accomplishment of the statistical analyses (MedCalc Software, Mariakerke, Belgium). To calculate the significance we used two-way ANOVA, Student's *t*-test (two-tailed) and Mann-Whitney *U*-test. The significance level was set at $p<0.05$ unless otherwise indicated. The presented data (mean±SD) are the results of at least three independent experiments.

Results and Discussion

In vitro cell culturing. A short-lived cell line could be developed from the bone marrow cells of leukemic Long-Evans rats, that could be directly re-transplanted to the experimental animals. In the suspension culture – created from the femoral bone marrow of the leukemic rats – the leukemic blast cells differentiated into *in vitro* non-dividing macrophages after 40±5 days (Figure 1).

In vitro [18F]F-FDG uptake studies. As part of the *in vitro* studies, we compared the [18F]F-FDG radiotracer accumulation in healthy control bone marrow cells and My1/De cells isolated from the bone marrow of leukemic Long-Evans rats and the tracer uptake by bone marrow-derived 20-day-old blast culture cell suspension.

The radiotracer uptake by the control cells gradually increased from the 15-min time point until the end of the experiment with corresponding values being 0.10±0.10, 0.24±0.12, and 0.49±0.16 at the 15-, 30-, and 60-min measurement points, respectively (Figure 2). Similarly, the My1/De bone marrow cell and the My1/De blast cell uptake of radioactivity also showed an increment from 15-60 min post-incubation.

Corresponding to the *in vitro* measurements of Trencsényi *et al*. with My2/De cells, the My1/De bone marrow cells exhibited more elevated [18F]F-FDG accumulation compared to the control bone marrow at all measurement points ($p\leq0.01$). The [18F]F-FDG uptake of the My1/De cells (blasts) was remarkably higher at all investigated time points than that of both the freshly isolated bone marrow cells ($p<0.01$) and the control cells. Although compared to the control cells, the radioactivity of the My1/De tumorous bone marrow cells appeared to be significantly more enhanced, their uptake values were below than those of the My1/De blast cell culture cells. The My1/De cell culture consisted of 100% tumor blast cells, while the tumorous bone marrow suspensions were made up by extremely heterogenous cell populations that have various glucose needs and metabolic activity. The difference between the glucose metabolism of the My1/De cell culture and the tumorous bone marrow suspensions may explain why the radiotracer uptake of the My1/De cells and the My1/De bone marrow differed. Figure 2 demonstrates the [18F]F-FDG uptake values (Panel A) and the tracer kinetics (Panel B) of the control and the My1/De bone marrow as well as the My1/De blast cells measured at different investigation points.

Table I. *[18F]F-FDG accumulation of selected organs and tissues in healthy control and myelomonoblastic leukemia 1 isolated at the University of Debrecen (My1/De) leukemic rats.*

	Control	My1/De
Muscle	0.80±0.08	0.97±0.07
Blood	0.51±0.09	0.48±0.05
Tumor (My1/De)	–	7.44±0.87
PTLN	0.94±0.34	4.25±0.28**
Thymus	1.41±0.25**	0.51±0.02
Spleen	1.67±0.05	3.71±0.26**
Liver	0.89±0.07	5.52±1.08**
Left kidney	2.30±0.36	5.37±0.13**
Right Kidney	2.14±0.47	2.21±0.58
Bone marrow	0.24±0.10	0.67±0.15*

Two weeks post SRCA operation, the study animals were euthanized and selected organs and tissues were harvested and weighed. The radioactivity was calculated by gamma-counting, and the results are presented in %ID/g units. Data are shown as mean±SD of at least three independent experiments. PTLN: Parathymic lymph node; SRCA: subrenal capsule assay. *$p<0.05$; **$p<0.01$.

Assessment of in vivo tumor propagation. To evaluate the primary tumor formation and metastatic spread of the subrenally transplanted My1/De cells, *in vivo* PET examinations were accomplished applying a preclinical PET device (MiniPET-II PET camera, University of Debrecen, Department of Medical Imaging, Division of Nuclear Medicine and Translational Imaging, Debrecen, Hungary). A representative PET image of a My1/De-carrying Long-Evans rat is presented in Figure 3.

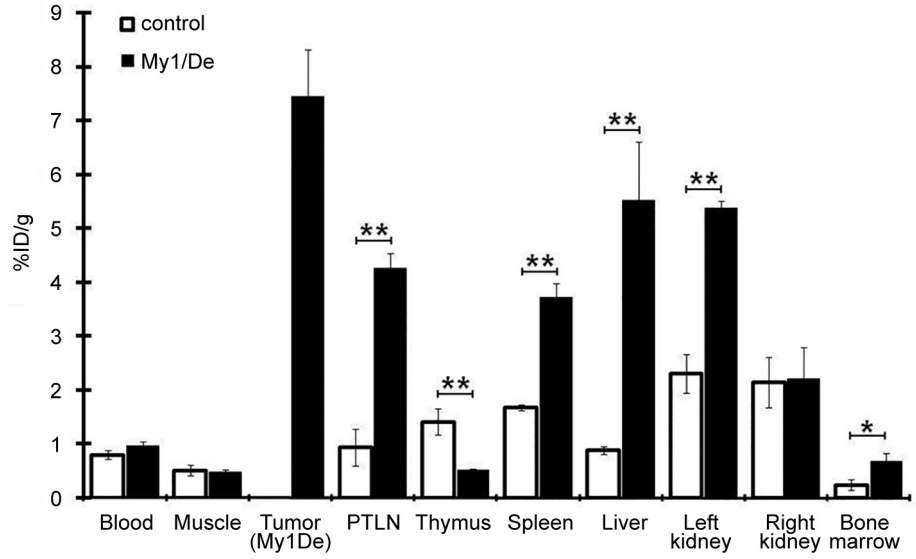

Figure 4. *[^{18}F]F-FDG uptake pattern of selected organs and tissues in healthy control and myelomonoblastic leukemia 1 isolated at the University of Debrecen (My1/De) leukemic rats. Two weeks post subrenal capsule assay operation, the study animals were euthanized, and selected organs and tissues were harvested and weighed. The radioactivity was calculated by gamma-counting, and the results are presented in %ID/g units. Data are shown as mean±SD of at least three independent experiments. PTLN: Parathymic lymph node; SD: standard deviation.*

Assessing the PET images of the experimental rats - performed two weeks post tumor implantation - we noted that the myeloblastic sarcoma started to grow and increase in size in the left kidney, and it reached a considerable volume at the time of PET imaging (as seen in Figure 3, black arrow). Accordingly, significant [^{18}F]F-FDG accumulation (SUV_{mean}: 9±1.7) was observed in the left renal region. As indicated in Figure 3, the left kidney could not be clearly delineated from the neighbouring tissues and organs, which was due to the infiltrative character of the tumor mass (Figure 3, black arrow). The *in vivo* dissemination of the My1/De cells from the primary tumor site to distant tissues and organs was tracked using PET imaging.

Tumor-related PTLN enlargement indicated that the subrenally developing primary tumors projected metastasis to the thoracic PTLNs (depicted in Figure 3, white arrow). Thus, corresponding enhanced [^{18}F]F-FDG uptake (SUV_{mean}: 6±1.4) was registered on both sides of the thorax. In a like manner, subrenally transplanted My2/De leukemia cells also propagated *via* the lymphatic channels, and generated metastasis in the thoracic PTLNs (18). In line with this, hepatocarcinoma (He/De) and mesoblastic nephroma (Ne/De) cells growing under the left renal capsule also appeared in the PTLNs by entering the intrathoracic lymphatic system (22-24). The finding of Tilney on the lymphatic drainage of rats (25), according to which the PTLNs receive lymph from the the peritoneal cavity, the pericardium, the liver, and the thymus through the lymph trunk of the mediastinum confirms the connection between the lymphatic vasculature of the left renal capsule and the PTLNs. Similarly to the leukemic cells, other colloid particles such as India Ink was also reported to be delivered to the thoracal lymphatic vessels and nodes *via* the transdiaphragmatic lymphatic channels (18, 26) which further strengthened the strong association of the renal and thoracal lymphatic system. In agreement with prior research studies (22, 26) we therefore may draw the conclusion that the kidney capsule-PTLN complex may be a valuable tool to explore *in vivo* tumor development and metastatic propagation.

In addition, hepatic and mesenterial lymph node expansion related to tumor infiltration resulted in significant tracer accretion in these regions as well (liver SUV_{mean}: 8±0.9; Figure 3, red arrow). The enlarged spleen was not well identifiable on the PET scans, which could presumably be due to the close proximity of the tumorous left kidney that occupied the majority of the abdominal cavity. The lack of meaningful radioactivity in other tissues/organs referred to the absence of spontaneous tumor development and the presence of inflammatory or infectious processes. Overall, My1/De cells growing under the left renal capsule induced leukemia in abdominal organs (left kidney, liver, spleen) and metastasized to the abdominal and thoracic lymph nodes (mesenteric and parathymic).

Ex vivo organ distribution studies. To evaluate the [^{18}F]F-FDG uptake pattern of the healthy and the My1/De tumor-carrying rats, *ex vivo* biodistribution studies were performed two weeks after the SRCA operations (seen in Figure 4). Significantly higher %ID/g values were observed in the liver,

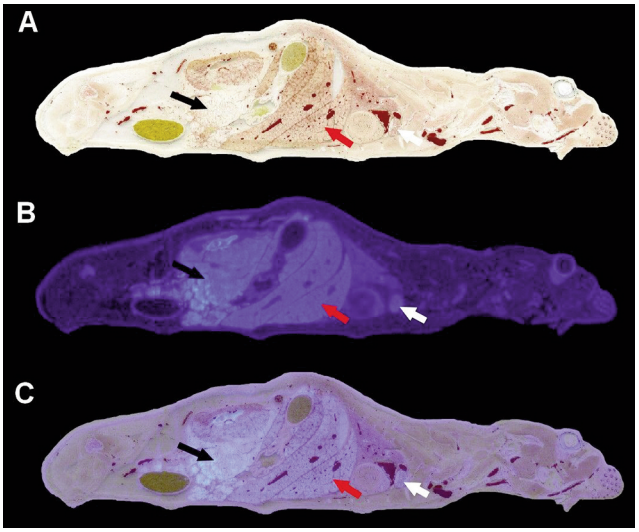

Figure 5. *Representative autoradiographic and anatomical sagittal sections of a myelomonoblastic leukemia 1 isolated at the University of Debrecen (My1/De) tumor-bearing Long-Evans rat. Whole-body autoradiographic section showing the [^{18}F]F-FDG uptake pattern of a My1/De tumor-bearing rat (Panel A). Corresponding anatomical section of a My1/De tumorous rat (Panel B). Panel C: merged image of A and B panels. The red arrow points to the liver, the white arrow indicates the metastatic parathymic lymph node (PTLN). The black arrow indicates the subrenally growing primary tumor.*

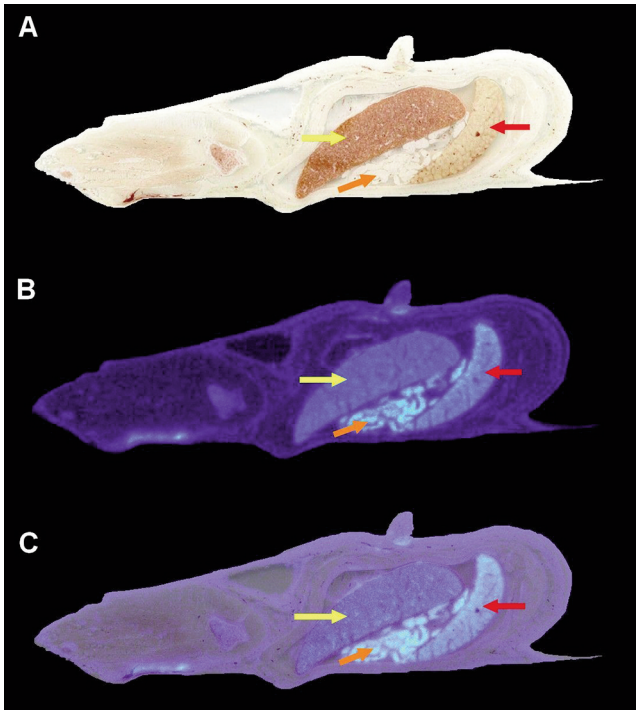

Figure 6. *Representative autoradiographic and anatomical sagittal sections of a parathymic lymph node (My1/De) tumor-bearing Long-Evans rat. Whole-body autoradiographic section showing the [^{18}F]F-FDG uptake pattern in a My1/De tumor-bearing rat (A). Corresponding anatomical section of a My1/De tumorous rat (B). C) merged image of A and B panels. The yellow, the red, and the orange arrows indicate the spleen, liver, and a metastatic mesenteric lymph node, respectively.*

spleen, left kidney, PTLN (p<0.01) and in the bone marrow (p<0.05) of the leukemic rats than in the same organs of the control rats, which could be attributed to the neoplastic infiltration of the listed organs. Thymic atrophy - induced by tumor-related stress - could explain the lower [^{18}F]F-FDG accumulation in the thymus of the tumorous rats compared to the control animals. In addition, no considerable difference was found between the radioactivity of the other assessed control and leukemic organs (the right kidney, blood, and the muscle tissue).

As demonstrated in Table I, the highest %ID/g value was recorded in the My1/De tumors of the leukemic rats (7.44±0.87), that was followed by the liver (5.52±1.08), the left kidney (5.37±0.13) and the PTLN (4.25±0.28). These findings were in line with the [^{18}F]F-FDG uptake values expressed in SUV. In contrast to our results, in a prior study of Trencsényi *et al*. on My2/De leukemic cells, the greatest [^{18}F]F-FDG accumulation was observed in the metastatic PTLNs of the tumor-bearing rats (18). The difference between the metastatic potential and the aggressiveness of the My1/De and the My2/De cells may suggest some explanations for the varying uptake figures.

We observed that the subrenally implanted myelomonoblastic sarcoma (My1/De) started to grow in the form of a solid tumor under the left renal capsule, and thereafter it showed systemic propagation, inducing tumor formation in several other organs. Although the left kidney was heavily invaded by the malignant cells, given its lower tracer accretion (5.37±0.13) relative to the tumor itself (7.44±0.87), we hypothesize the presence of intact, functioning renal parenchyma in the left kidney besides the neoplastic tissue. Table I exhibits the [^{18}F]F-FDG %ID/g values of the investigated organs/tissues and the My1/De tumor. The %ID/g value of the My1/De tumor appeared to be approximately seven-fold-higher compared to that of the muscle, which is used as a standard.

Whole-body autoradiography examinations. The tumorigenic and metastatic potential of the My1/De cells were assessed with whole-body autoradiography and phosphorimage analyses as well by transplanting 10^6 My1/De cells under the left renal capsule of Long-Evans rats. Followed by image analysis and the quantification of the pixel information of the scans, we calculated the relative intensity values of selected organs/tissues relative to the background muscle.

In line with the organ distribution results, the highest activity was observed for the subrenally growing

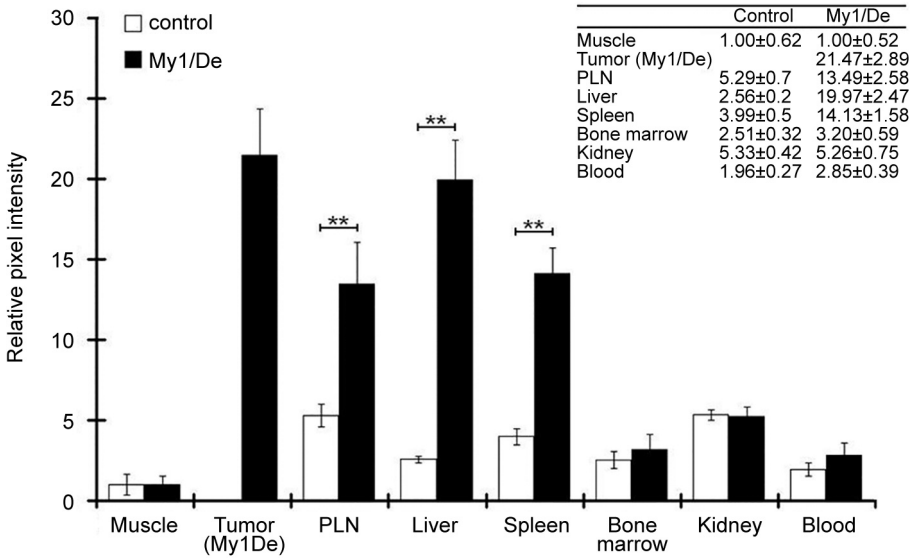

	Control	My1/De
Muscle	1.00±0.62	1.00±0.52
Tumor (My1/De)		21.47±2.89
PLN	5.29±0.7	13.49±2.58
Liver	2.56±0.2	19.97±2.47
Spleen	3.99±0.5	14.13±1.58
Bone marrow	2.51±0.32	3.20±0.59
Kidney	5.33±0.42	5.26±0.75
Blood	1.96±0.27	2.85±0.39

Figure 7. *Relative intensity distribution post intravenous injection of [^{18}F]F-FDG in the autoradiographic image of myelomonoblastic leukemia 1 isolated at the University of Debrecen (My1/De) tumor-carrying Long Evans rats; The values were normalized to the muscle.*

Table II. *Percentage distribution of the peripheral white blood cells of healthy control and myelomonoblastic leukemia 1 isolated at the University of Debrecen (My1/De) leukemic Long-Evans rats.*

	Control	My1/De Myelomonoblastic leukemia
WBC count (g/l)	6-7	60-80
Metamyelocyte	3%	0%
Neutrophil granulocyte	26%	15%
Eosinophil granulocyte	2%	1%
Lymphocyte	66%	7%
Monocyte	3%	1%
Blast	0%	50-80%

Subrenal capsule assay was used for the inoculation of 10^6 My1/De cells under the left renal capsule of 10 Long-Evans rats. Two weeks post transplantation all rats were euthanized, and peripheral blood was taken for white blood cell (WBC) count determination and the assessment of the distribution of the different WBC subtypes.

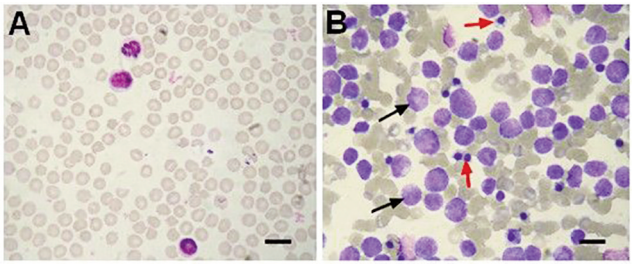

Figure 8. *Wright-Giemsa staining of myelomonoblastic leukemia 1 isolated at the University of Debrecen (My1/De) cells isolated from the peripheral blood of control (A) and My1/De leukemic (B) Long-Evans rats. Subrenal capsule assay experimental operation was used for the inoculation of 10^6 My1/De cells under the left renal capsule of 10 Long-Evans rats. Two weeks post transplantation all rats were euthanized, and Wright-Giemsa-stained smears were prepared from the peripheral blood of the control (A) and the My1/De leukemic (B) Long-Evans rats. black arrow: blast cells; red arrow: nucleated red blood cell. Wright-Giemsa staining. Indication: 10 μm. (Original magnification ×1,000).*

myelomonoblastic tumor (seen in Figure 5, black arrows). Owing to infiltration by leukemic blast cells, the metastatic PTLNs (Figure 5, white arrows) and mesenteric lymph nodes (Figure 6, orange arrow), the liver (Figure 5 and Figure 6, red arrows), and the spleen (Figure 6, yellow arrows) also expressed outstanding activity compared to the control (Figure 7). These findings are supported by the *ex vivo* [^{18}F]F-FDG uptake values presented in %ID/g. In addition, lower intensity values were recorded for the bone marrow as expected.

In summary, the major finding of the autoradiography experiment is that the subrenally developing tumors primarily metastasize to the PTLNs.

Microscopic and macroscopic analyses of leukemic rat-derived samples. Peripheral smears. Cytochemical staining was used to verify the leukemic origin of cells obtained from the peripheral blood of My1/De leukemic rats. Two weeks after the subrenal transplantation of the My1/De cells, the WBC count in the peripheral smear of the leukemic Long-

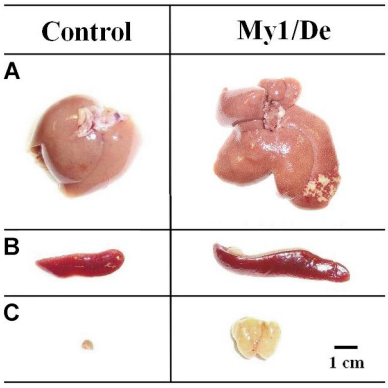

Figure 9. *Presentation of control and leukemic organs removed two weeks after SRCA operation. Myelomonoblastic leukemia 1 isolated at the University of Debrecen (My1/De) leukemic cells (10^6) were implanted under the left renal capsule of Long-Evans rats using the subrenal-capsule assay (SRCA) technique. Two weeks post SRCA transplantation, the experimental animals were sacrificed, and dissected. Leukemia-related organs were removed and compared. A) control liver, B) control spleen, C) control parathymic lymph node (PTLN), D) enlarged liver (hepatomegaly), E) enlarged spleen (splenomegaly), F) enlarged PTLN (lymphadenomegaly).*

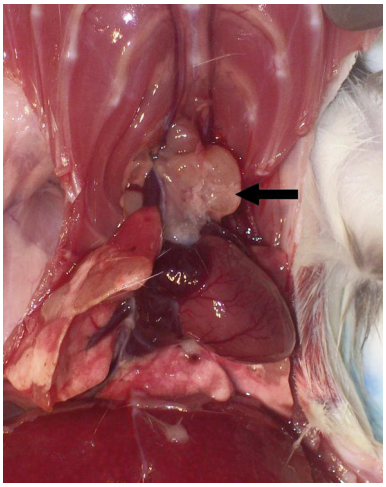

Figure 10. *Metastatic parathymic lymph node (PTLN) (black arrow) in the thorax two weeks after subrenal capsule assay-based tumor induction. The tumor-infiltrated, enlarged PTLNs (black arrow) occupied a large portion of the thorax.*

Table III. *Organ weight of the healthy control and My1/De tumorous rats.*

Organ	Control (%)	My1/De (%)
Liver	4.2±0.3	8.6±1.2
Spleen	0.2±0.05	0.8±0.07
Thymus	0.1±0.02	–
Left kidney	0.4±0.02	–
PTLN	0.008±0.001	0.2±0.07

10^6 My1/De cells (leukemic) were implanted under the left renal capsule of Long-Evans rats using the subrenal-capsule assay (SRCA). Two weeks post SRCA transplantation, the study animals were sacrificed, and dissected. The weight of the selected organs was measured and expressed as a percentage in relation to the total body weight of the animal. PTLN: Parathymic lymph node.

Evans rats showed a significant increase from 6-7 g/l to 60-80 g/l (as demonstrated in Table II). Blasts made up 50-80% of the WBCs in the sample of the tumor-bearing rats. Out of the WBC subtypes, the number of the lymphocytes presented the greatest decrease compared to the control cohort (from 66% to 7%, $p \leq 0.01$) (Table II). Table II displays the percentage distribution of the different types of WBCs.

Giemsa dye-stained leukemic blast cells in the blood were clearly identifiable in the peripheral smears of the tumorous rats (Figure 8, Panel B, back arrows). In addition, the peripheral smears provide a correct representation of nucleated red blood cells (NRBCs) in the different stages of maturation (Figure 8, Panel B, red arrows).

Autopsy. Two weeks post SRCA operation, healthy control and My1/De tumor-carrying rats were sacrificed. To compare the macroscopic and microscopic characteristics of leukemia-afflicted organs, the liver, the spleen, the bone marrow and the PTLNs of the rats were removed, sectioned and histological smears were prepared.

Autopsy findings revealed meaningful differences regarding the appearance and the weight of the selected organs (Figure 9 and Table III). Upon macroscopic analysis, an enlarged, lighter-coloured liver (hepatomegaly, Figure 9, Panel A), coupled with an enlarged spleen (splenomegaly, Figure 9, Panel B) and PTLN (lymphadenomegaly, Figure 9, Panel C) was observed for the My1/De tumor-carrying animals compared to their tumor-naïve counterparts. The tumor-infiltrated PTNs occupied a large portion of the thorax (Figure 10). Additionally, the normal parenchyma of the tumorous left kidney could not be obviously delineated from the tumor mass. Similarly to our results, another subrenally transplanted leukemic cell type - namely My2/De - also generated hepatic, splenic and parathymic nodal enlargement four weeks post SRCA operation (18). Based on autopsy findings, the My1/De cells show a greater proliferation rate compared to the My2/De cells, that may possibly indicate a more aggressive character and a worse prognosis for My1/De leukemia compared to the My2/De one. Figure 9 presents the macroscopic comparison of the assessed organs/tissues.

Followed by the extraction and the measurement of the control and tumorous organs, their weight relative to the animal body weight were determined (Table III). Remarkable differences were observed between the volume of the investigated organs. The parathymic lymph node (~1,300%)

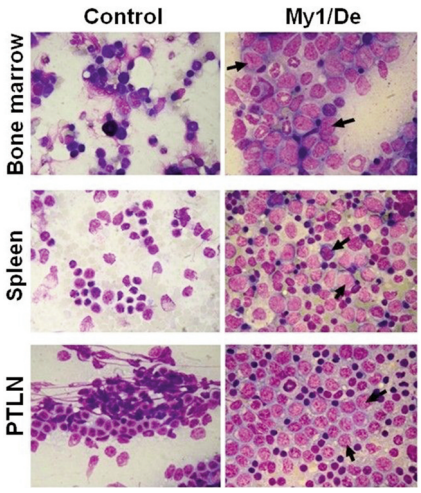

Figure 11. *Wright-Giemsa staining of myelomonoblastic leukemia 1 isolated at the University of Debrecen (My1/De) cells isolated from organs of healthy control and My1/De leukemic Long-Evans rats. 10^6 My1/De cells (leukemic) were implanted under the left renal capsule of Long-Evans rats using SRCA technique. Two weeks post transplantation all rats were euthanized. Thereafter the bone marrow, the spleen and the parathymic lymph node (PTLN) were extracted to prepare Wright-Giemsa-stained histological sections. A) Giemsa-stained healthy control bone marrow. (D) Bone marrow cells originated from leukemic rats. The black arrows indicate monoblasts. B) Giemsa-staining of control spleen cells. E) My1/De leukemic cells from the spleen. Monoblast cells are indicated by the black arrows. C) Giemsa-staining of control PTLN cells. F) My1/De leukemic cells from the PTLN. The black arrows indicate monoblasts. (original magnification: ×400).*

showed the greatest weight increase, that was followed by the spleen (~25%) and the liver (~35%) (Table III). In accordance with these findings, autopsy results on My2/De leukemia-bearing rats showed similar tendency regarding organ growth *(PTLN>spleen>liver)* (18). Although the similarity between the organ weight increase of the My1/De and My2/De tumorous rats would project identical [^{18}F]F-FDG uptake in the assessed organs, significant differences were experienced in their radioactivity, that could be due to the variance between the viability or the metabolic activity of the My1/De and My2/De cells.

As exhibited in Figure 11, Wright-Giemsa-stained smears from the bone marrow, spleen and PTLNs were prepared. In accordance with the macroscopic analysis, the evaluation of the post-mortem histological sections also confirmed the leukemic involvement of the organs (Figure 11). The Wright-Giemsa-stained sections revealed leukaemia-related hypercellularity with a large number of blasts in all leukemic aspirate smears (Figure 11). The blast cells are characterised by large, either eccentric or centrally placed, round-shaped nucleus with a few nucleoli. The nucleus is surrounded by basophilic and slightly granulated cytoplasm. The presence of RBCs at various stages of differentiation in the splenic smears from both the control and the leukemic rats is physiological, since the spleen has major role in erythropoiesis in adult rats.

Conclusion

With the aim of extending knowledge on AML pathophysiology, a preclinical My1/De rat model was successfully developed. Indicating lymphatic spread of metastasis, the subrenally implanted My1/De cells developed metastasis to the thoracic PTLNs and the mesenterial lymph nodes. Overall, the translation of the currently established My1/De model into advanced *in vivo* preclinical and clinical stages of research may open avenue for the further analyses of leukemia development that might have human implications in terms of therapeutic management.

Funding

No funding.

Conflicts of Interest

The Authors declare no conflicts of interest in relation to this study.

Authors' Contributions

Conceptualization: Gy.T.; Data curation: G.O., I.J.; Investigation: V.A., J.P.Sz., G.F., N.D., A.K.; Methodology: Z.K., I.H., Gy.T., I.K.; Validation: Z.K., G.O.; Visualization: Gy.T.; Writing original draft: Z.K., Gy.T.; Writing review & editing: Z.K., Gy.T., I.K. All Authors have read and agreed to the published version of the manuscript.

Acknowledgements

This study was supported by the ÚNKP-23-4-II new national excellence program of the ministry for culture and innovation from the national research, development and innovation fund and supported by the ÚNKP-23-5 new national excellence program of the ministry for culture and innovation from the source of the national research, development and innovation fund. The research was also supported by the Hungarian National Research, Development and Innovation Office (FK-134551 project).

References

1 Turkalj S, Radtke FA, Vyas P: An overview of targeted therapies in acute myeloid leukemia. Hemasphere 7(6): e914, 2023. DOI: 10.1097/HS9.0000000000000914

2 Skayneh H, Jishi B, Hleihel R, Hamieh M, Darwiche N, Bazarbachi A, El Sabban M, El Hajj H: A critical review of animal models used in acute myeloid leukemia pathophysiology. Genes (Basel) 10(8): 614, 2019. DOI: 10.3390/genes10080614

3 Cyagen, Technical Bulletin, Newsletter, Research Trend: Rats - The Animal Model that is Revitalizing Medical Research 2020: Available at: https://www.cyagen.com/us/en/community/technical-bulletin/rat-model.html [Last accessed on February 20, 2024]

4 Zhao S, Shetty J, Hou L, Delcher A, Zhu B, Osoegawa K, de Jong P, Nierman WC, Strausberg RL, Fraser CM: Human, mouse, and rat genome large-scale rearrangements: stability *versus* speciation. Genome Res 14(10A): 1851-1860, 2004. DOI: 10.1101/gr.2663304

5 Svejda J, Kossey P, Hlavayova E, Svec F: Histological picture of the transplantable rat leukaemia induced by x-irradiation and methylcholanthrene. Neoplasma 5(2): 123-131, 1958.

6 Huggins CB, Sugiyama T: Induction of leukemia in rat by pulse doses of 7, 12-dimethylbenz (a) anthracene. Proc Natl Acad Sci USA 55(1): 74-81, 1966.

7 Huggins CB, Grand L, Ueda N: Specific induction of erythroleukemia and myelogenous leukemia in Sprague-Dawley rats. Proc Natl Acad Sci USA 79(17): 5411-5414, 1982.

8 Gross L: Induction of leukemia in rats with mouse leukemia (passage A) virus. Proc Soc Exp Biol Med 106(4): 890-893, 1961. DOI: 10.3181/00379727-106-26512

9 Metcalf RG, Inda FA: Pathology in animals subjected to repeated daily exposure to X-rays. In: Biological effects of external radiation. Blair HA (ed.). New York City, NY, USA, Mc Graw-Hill, pp. 268-338, 1954.

10 Shay H, Gruenstein M, Marx HE, Glazer L: The development of lymphatic and myelogenous leukemia in Wistar rats following gastric instillation of methylcholanthrene. Cancer Res 11(1): 29-34, 1951.

11 Van Bekkum DW, Hagenbeek A: Relevance of the BN leukemia as a model for human acute myeloid leukemia. Blood Cells Mol Dis 3(3): 565-579, 1977.

12 Martens AC, Van Bekkum DW, Hagenbeek A: The BN acute myelocytic leukemia (BNML) (a rat model for studying human acute myelocytic leukemia (AML)). Leukemia 4(4): 241-257, 1990.

13 Nooter K, Sonneveld P, Deurloo J, Oostrum R, Schultz F, Martens A, Hagenbeek A: Repeated daunomycin administration in rats. Cancer Chemother Pharmacol 12(3): BF00256543, 1984. DOI: 10.1007/BF00256543

14 Ermens AA, Kroes AC, Lindemans J, Abels J: 5-Fluorouracil treatment of rat leukemia and a reappraisal of its application in human leukemia. Anticancer Res 6(4): 797-800, 1986.

15 Sonneveld P, Holcenberg JS, Van Bekkum DW: Effect of succinylated Acinetobacter glutaminase-asparaginase treatment on an acute myeloid leukemia in the rat (BNML). Eur J Cancer (1965) 15(8): 1061-1063, 1979. DOI: 10.1016/0014-2964(79)90294-9

16 Greenberger JS, Bocaccino CA, Szot SJ, Moloney WC: Chemotherapeutic remissions in Wistar Furth rat acute myelogenous leukemia: a model for human AML. Acta Haematol 57(4): 233-241, 1977. DOI: 10.1159/000207886

17 Gál F, Somfai S, Szentirmay Z: Transplantable myeloid rat leukaemia induced by 7,12-Dimethylbenz(a)anthracene. Acta Haematol 49(5): 281-290, 1973. DOI: 10.1159/000208415

18 Trencsenyi G, Nagy G, Kahlik B, Nemeth E, Kertai P, Kiss A, Banfalvi G: Lymphoid metastasis of rat My2/De leukemia. Leuk Res 38(5): 586-593, 2014. DOI: 10.1016/j.leukres.2014.02.006

19 Workman P, Aboagye EO, Balkwill F, Balmain A, Bruder G, Chaplin DJ, Double JA, Everitt J, Farningham DA, Glennie MJ, Kelland LR, Robinson V, Stratford IJ, Tozer GM, Watson S, Wedge SR, Eccles SA, Committee of the National Cancer Research Institute: Guidelines for the welfare and use of animals in cancer research. Br J Cancer 102(11): 1555-1577, 2010. DOI: 10.1038/sj.bjc.6605642

20 Trencsenyi G, Kertai P, Bako F, Hunyadi J, Marian T, Hargitai Z, Pocsi I, Muranyi E, Hornyak L, Banfalvi G: Renal capsule-parathymic lymph node complex: a new *in vivo* metastatic model in rats. Anticancer Res 29(6): 2121-2126, 2009.

21 Képes Z, Trencsényi G: Subrenal capsule assay - SRCA: The promising re-emergence of a long-forgotten method in preclinical nuclear medical cancer diagnostics. J Cancer 14(2): 183-192, 2023. DOI: 10.7150/jca.78599

22 Banfalvi G: Role of parathymic lymph nodes in metastatic tumor development. Cancer Metastasis Rev 31(1-2): 89-97, 2012. DOI: 10.1007/s10555-011-9331-y

23 Szabo JP, Denes N, Arato V, Racz S, Kis A, Opposits G, Kepes Z, Hajdu I, Joszai I, Emri M, Kertesz I, Mezo G, Trencsenyi G: *In vivo* imaging of neo-angiogenesis of transplanted metastases in subrenal capsule assay induced rat model. In Vivo 36(4): 1667-1675, 2022. DOI: 10.21873/invivo.12878

24 Szabó JP, Csige K, Kálmán-Szabó I, Arató V, Opposits G, Jószai I, Kertész I, Képes Z, Méhes G, Fenyvesi F, Hajdu I, Trencsényi G: *In vivo* assessment of tumor targeting potential of 68Ga-labelled randomly methylated beta-cyclodextrin (RAMEB) and 2-hydroxypropyl-β-cyclodextrin (HPβCD) using positron emission tomography. Int J Pharm 630: 122462, 2023. DOI: 10.1016/j.ijpharm.2022.122462

25 Tilney NL: Patterns of lymphatic drainage in the adult laboratory rat. J Anat 109(Pt 3): 369-383, 1971.

26 Rozsa D, Trencsenyi G, Kertai P, Marian T, Nagy G, Banfalvi G: Lymphatic spread of mesenchymal renal tumor to metastatic parathymic lymph nodes in rat. Histol Histopathol 24(11): 1367-1379, 2009. DOI: 10.14670/HH-24.1367

Received January 14, 2024
Revised February 19, 2024
Accepted February 20, 2024